Biophysical Journal, Volume *122*

Supplemental information

NAD(P)H binding configurations revealed by time-resolved fluorescence and two-photon absorption

Thomas S. Blacker, Michael R. Duchen, and Angus J. Bain

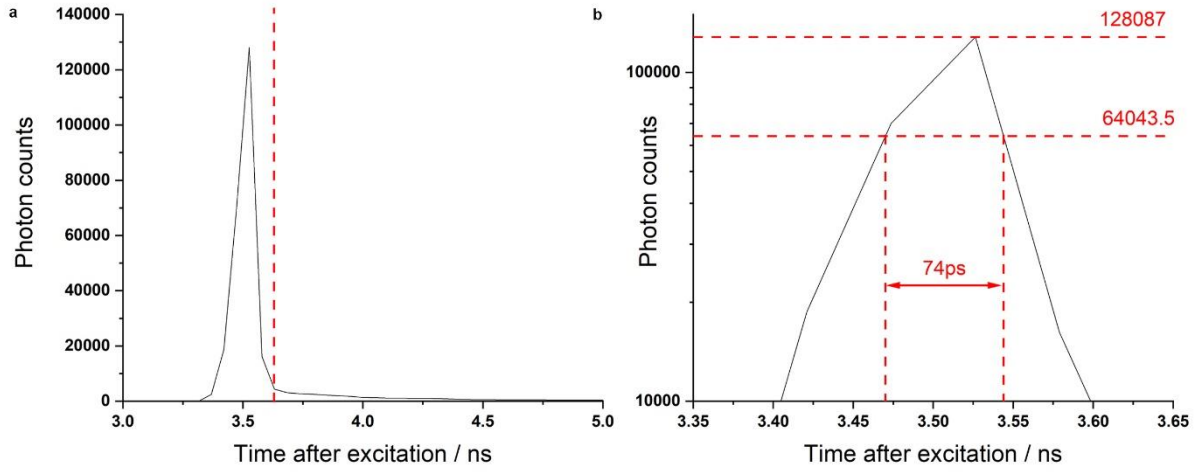

Figure S1: The instrument response function (IRF) associated with our measurements was determined by performing TCSPC at 340nm on NADH added to a saturated solution of potassium iodide, a highly effective quencher(1). This revealed the FWHM of the response to be 74ps. A small tail after the peak (from 3.6ns onwards) could be fit to a biexponential decay with decay constants of 0.47(±0.02) ns and 4.0(±0.1) ns with relative amplitudes of 99.98(±0.01)% and 0.02(±0.01)%. This suggested it to originate primarily from residual unquenched NADH with a characteristic lifetime of 0.4-0.5ns. The longer lifetime minority species may have originated from the potassium iodide itself, which can absorb in the near-UV and fluoresce in the 364-600nm emission window utilised(2).

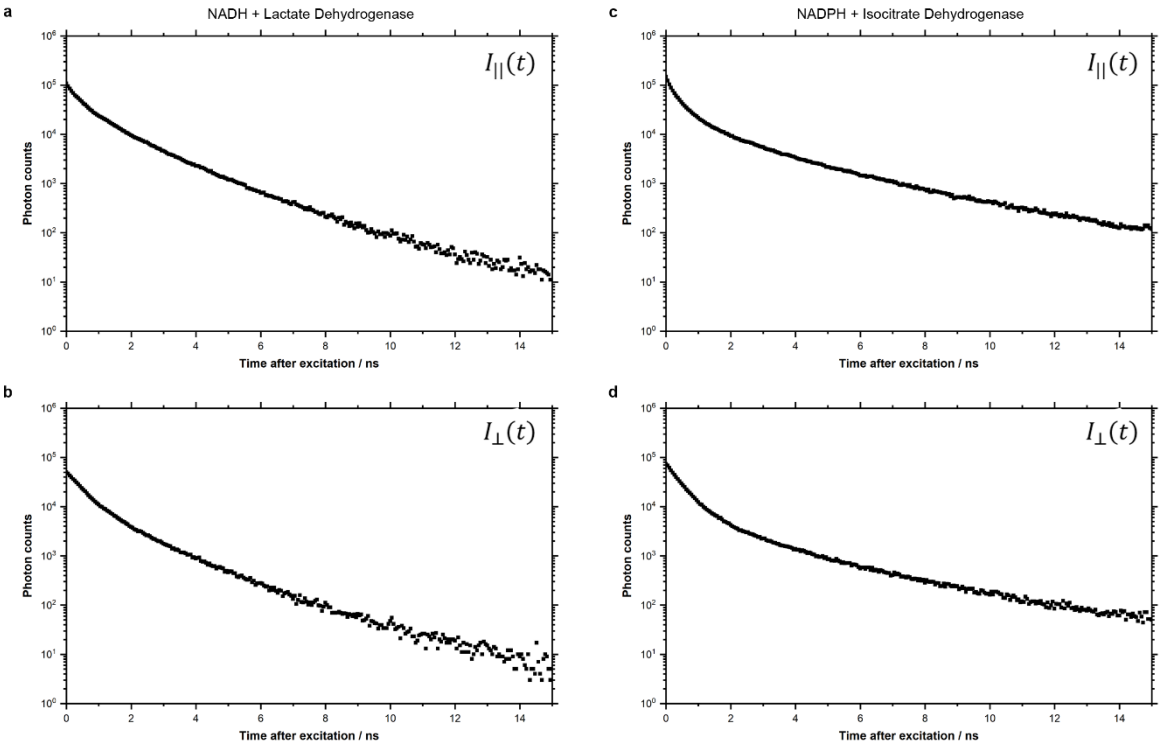

Figure S2: The polarised fluorescence decays $I_{||}(t)$ and $I_{\perp}(t)$, from which the total intensity $I(t)$ and anisotropy $R(t)$ decays were calculated using Equations 1 and 3, for (a & b) NADH mixed with lactate dehydrogenase and (c & d) NADPH mixed with isocitrate dehydrogenase.

Appendix S1

Maximum likelihood fitting of two-photon fluorescence intensity decays

Despite least-squares global fits to the two-photon fluorescence intensity decays giving low χ_R^2 values, the residuals were systematically offset from zero (Figure S3). This suggested an underlying discrepancy between the fitting model and the experimental data, reducing our confidence in the accuracy of the fluorescence decay parameters extracted. This could result from the variance of the data points being improperly assigned in the least-squares weighting function, despite this method being successful in the single-photon case. A known drawback of the least-squares approach described in the main text is that Equation 5 assumes that the Poisson statistics describing photon counting data can be approximated as Gaussian(3). However, this only applies when the number of photon counts in each bin is above approximately 10(4, 5), as shown in Figure S4.

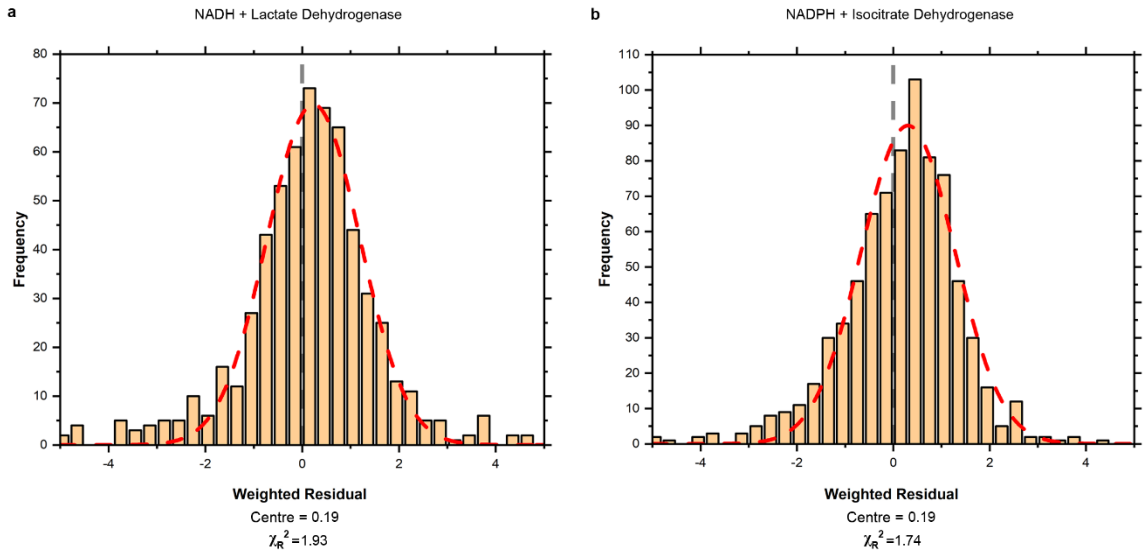

Figure S3: Least-squares fits of a three-component decay model were systematically offset from the time-resolved two-photon fluorescence data. These global fits, in which the three lifetimes were shared between the datasets obtained using linearly and circularly polarised excitation, resulted in acceptable χ_R^2 values. However, the arithmetic means of the weighted residuals were offset from zero, suggesting the fit parameters may be inaccurate.

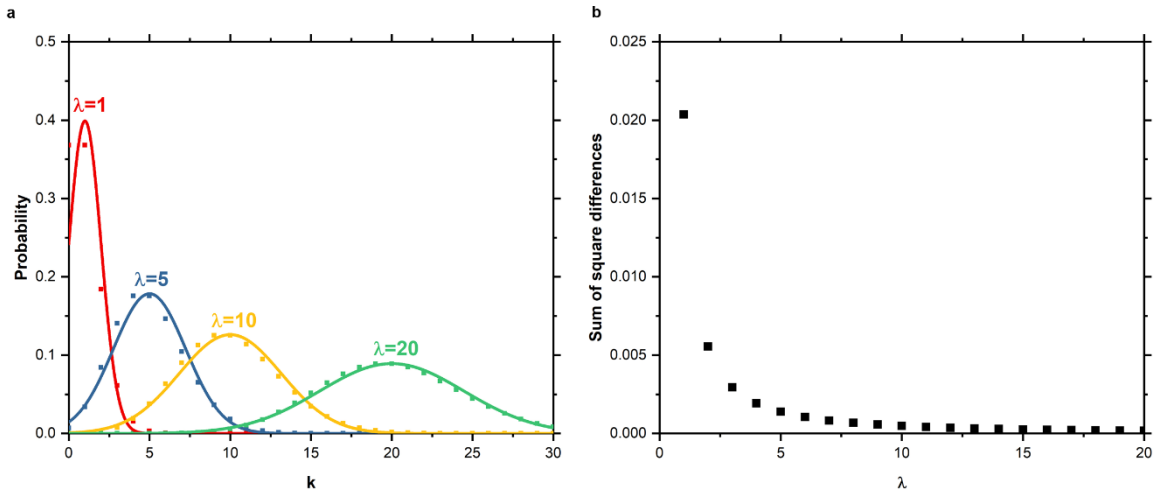

Figure S4: (a) A comparison of the Poisson (points) and Gaussian (lines) distributions, describing the probability of measuring k counts for an expected occurrence rate λ. The similarity of the two distributions increases with λ, as quantified in (b) by the sum of square differences between the distributions.

The lower count rates resulting from two-photon excitation combined with the extended (27ns) excitation-emission correlation times available with our apparatus resulted in 34% of the bins containing fewer than 10 counts, in contrast to 0% with single-photon excitation. To account for this, the maximum likelihood approach can be applied(3, 6–8). Here the fitting algorithm aims to minimise a χ_R^2 based on the likelihood function,

$$\chi_R^2 = \frac{2}{n-l}\sum_{k=1}^{n}\left\{I_{\text{measured}}(t_k)\ln\left[\frac{I_{\text{measured}}(t_k)}{I_{\text{model}}(t_k)}\right] - [I_{\text{measured}}(t_k) - I_{\text{model}}(t_k)]\right\} \quad \text{(S1)}$$

with the magnitude of the residuals given by,

$$|x_k| = \sqrt{2\left\{I_{\text{measured}}(t_k)\ln\left[\frac{I_{\text{measured}}(t_k)}{I_{\text{model}}(t_k)}\right] - [I_{\text{measured}}(t_k) - I_{\text{model}}(t_k)]\right\}} \quad \text{(S2)}$$

and their sign reflecting $I_{\text{measured}}(t_k) - I_{\text{model}}(t_k)$.

This method will underestimate the variance of each datapoint in our experiments as our $I(t)$ data is reconstructed from the addition of polarised decays according to Equation 1, not from

single magic angle measurements. This renders the statistics of the datasets non-Poissonian resulting in the return of quantitatively incorrect χ_R^2 values and preventing the calculation of 95% confidence intervals as per the least squares fits. Quoted uncertainties (see Table S1) are therefore standard deviations calculated from the variance-covariance matrix, which will underestimate the true confidence intervals. Nevertheless, this approach now provided fits with evenly distributed residuals (Figure S5), thereby correcting for the unsatisfactory fits obtained with least squares methods.

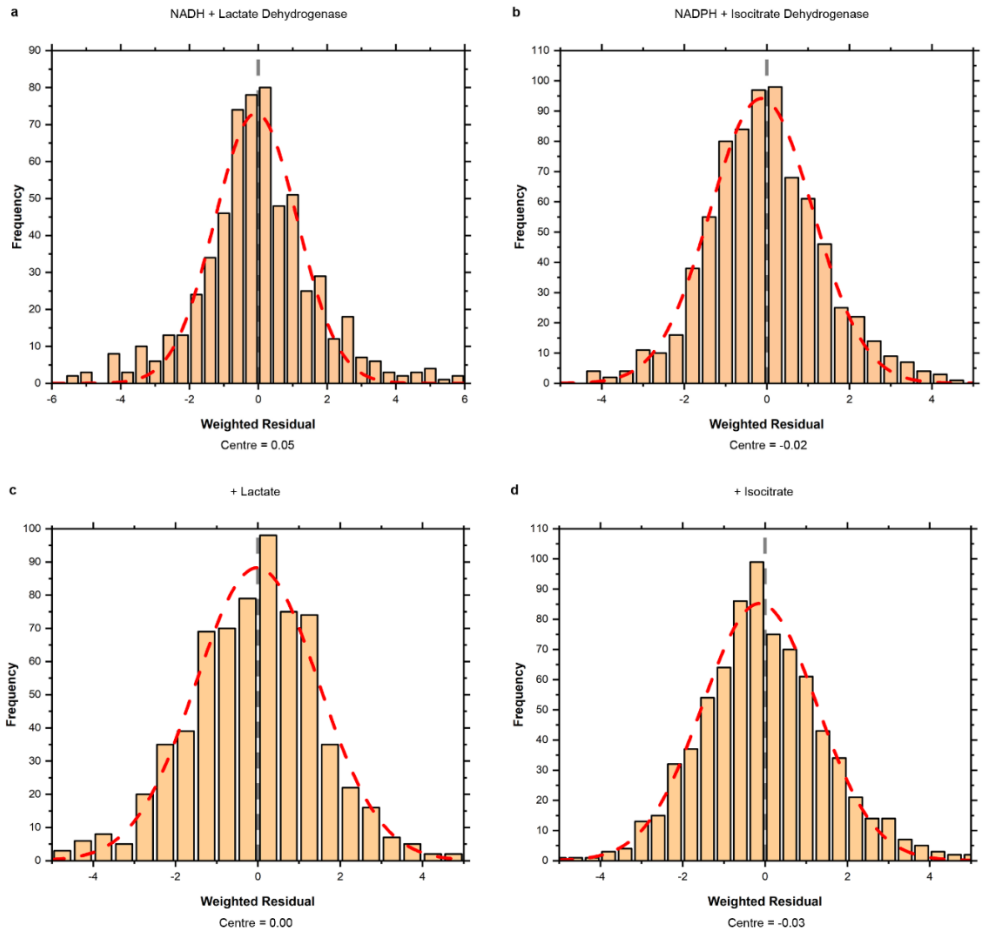

Figure S5: Maximum likelihood fitting to the experimental two-photon fluorescence decay data improved the distribution of the residuals in comparison to weighted least-squares. The likelihood function will underestimate the variance of the data as I_V and I_H were obtained separately in our experiments, meaning the absolute values of χ_R^2 associated with Equation S1 will be larger than their true value.

Appendix S2

Rejection of alternative models for the anisotropy decay of NAD(P)H enzyme mixtures

To confirm the validity of the model described by Equation 16, we compared its performance with both simpler and more complex models. First, we assessed a model in which local motion of the nicotinamide was neglected, with the free species exhibiting a fast rotational correlation time and the two bound species sharing a slower rotational correlation time,

$$R(t) = \frac{R(0)}{\alpha_1 e^{-t/\tau_1} + \alpha_2 e^{-t/\tau_2} + \alpha_3 e^{-t/\tau_3}} \Big(\alpha_1 e^{-t/\tau_1} e^{-t/\tau_{\text{fast}}^{\text{rot}}} + e^{-t/\tau_{\text{slow}}^{\text{rot}}} \{ \alpha_2 e^{-t/\tau_2} + \alpha_3 e^{-t/\tau_3} \} \Big) \tag{S3}$$

Fitting of this model gave evenly distributed residuals, but poorer values of χ_R^2 in comparison to the local motion model, at 3.09 for NADH and lactate dehydrogenase and 3.11 for NADPH and isocitrate dehydrogenase. Furthermore, it performed poorly when assessing the physical validity of the parameters output. $\tau_{\text{slow}}^{\text{rot}}$ was 55(±9) ns for lactate dehydrogenase and 160(±40) ns for isocitrate dehydrogenase. By the Stokes-Einstein-Debye equation, the ratio of these correlation times should follow(9),

$$\frac{\tau_{\text{slow}}^{\text{IDH}}}{\tau_{\text{slow}}^{\text{LDH}}} = \frac{(f\kappa V_h)_{\text{IDH}}}{(f\kappa V_h)_{\text{LDH}}} \tag{S4}$$

The form factor f is 1 for a sphere and deviates above or below this value for increasingly non-spherical shapes. κ varies between 0 and 1 depending on the degree of interaction between protein and solvent. Assuming equal protein densities, the ratio of hydrodynamic volumes for isocitrate dehydrogenase to lactate dehydrogenase can be approximated to their molecular weight ratio of 1.3, whereas the ratio of slow rotational correlation times here was 2.5(±0.5). It is unlikely that κ will differ drastically between the two enzymes, as all proteins are typically surrounded by an extended hydration shell(10). Furthermore, crystal structures of lactate

dehydrogenase and isocitrate dehydrogenase(11, 12) do not imply either has a highly oblate or prolate form ($f \sim 1$). Equation S3 therefore produced physically unrealistic results. In contrast, the ratio of slow rotational correlation times output by the model that accounted for local motion of the nicotinamide (Equation 16) was 1.3(±0.7), in agreement with their ratio of molecular weights, supporting its validity.

The satisfactory fits by Equation 16 implied that the initial anisotropy is equal for each species close to the theoretical maximum of 0.4. To confirm this, we altered this model to include a separate $R(0)$ for each component of the decay. This did not alter the χ_R^2 for the fit, thereby providing no statistical justification for accepting this more complex model. Furthermore, the resulting initial anisotropies were essentially unchanged, with values of 0.38(±0.01) and 0.39(±0.01) for the free species in the NADH and NADPH mixtures respectively, and 0.40(±0.01) for each bound species. While this may imply that a small difference between the absorption and emission transition dipole moments in the free cofactor is eliminated by enzyme binding, this cannot be fully confirmed at the current level of experimental accuracy.

Appendix S3

Identification of potential artefacts induced by tail fitting of decay data

To critically assess the use of the "tail fitting" approach, we performed numerical simulations in MATLAB (The MathWorks, Natick MA, USA). The population and rotational decay dynamics associated with the NADH and lactate dehydrogenase mixture (see Tables 1 and 2) were used to generate separate polarised fluorescence decays using,

$$I_{||}(t) = \frac{I(t)}{3}[1 + 2R(t)] \tag{S5}$$

$$I_{\perp}(t) = \frac{I(t)}{3}[1 - R(t)] \tag{S6}$$

These were each convolved with Gaussian IRFs with FWHMs varying from 0 to 200ps, scaled such that $I_{\max} = 207691$ (to reflect our experimental measurements) and Poisson noise added using the poissrnd() command. The decays were then fit in the manner described in the Methods section. This was repeated 100 times at each FWHM and the results compared with the underlying decay parameters, displayed in Figure S6.

The average intensity decay amplitudes were close (with 3%) to their true values at all IRF widths. This was also the case for the two shorter fluorescence lifetimes τ_1 and τ_2, the means of the 100 repeats being at most 85ps from the underlying value. The spread of τ_3 values returned was much larger than the other intensity decay parameters (at most 550ps), presumably because of its small amplitude and therefore low contribution to the overall signal. As such, at two IRF widths, the average τ_3 value returned was well above (0.8-0.9ns) the true value. However, this appeared unlikely to be a systematic effect of tail fitting given it occurred at a FWHM of 125ps but not 150ps or 175ps, and the lifetime in question was over 15 times larger than these values.

The distinction in restricted rotational diffusion between the two bound species ($B_2 > B_3$) could be identified at all IRF widths. In each case, B_3 was correctly assigned as zero. The mean values of B_2 were slightly lower than the true underlying value. Up to a FWHM of 125ps, these averaged 0.155 relative to the true value of 0.17, with which the spread of each dataset overlapped. A systematic underestimate of B_2 may be evident beyond these values. This could be associated with a systematically underestimated correlation time associated with this motion at IRF widths of 125ps and above and overestimates of the correlation time of unbound species which increased from 0.15ns above the true value at a FWHM of 125ps to 0.28ns at 200ps.

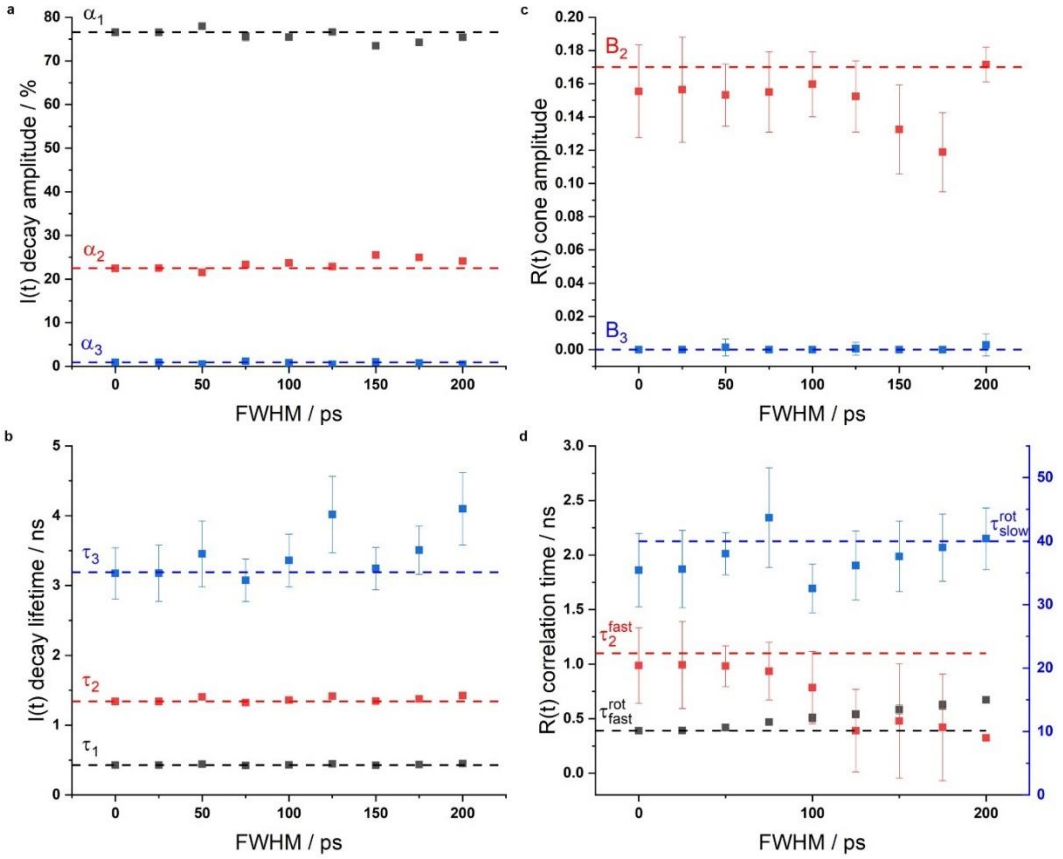

Figure S6: Parameters obtained by tail fitting 100 simulated intensity and anisotropy decay datasets at different Gaussian IRF widths. Dashed lines represent the true underlying parameters.

Table S1

Polarised two-photon fluorescence parameters of NADH mixed with lactate dehydrogenase and NADPH mixed with isocitrate dehydrogenase, and in ternary complexes

	NADH+LDH	+ Lactate	NADPH+IDH	+ Isocitrate
$\overline{\Omega}$	1.04(±0.01)	1.07(±0.01)	0.94(±0.01)	0.97(±0.01)
τ_1 / ns	0.2(±0.4)	0.2(±0.3)	0.26(±0.04)	0.2(±0.3)
τ_2 / ns	1.1(±0.1)	1.3(±0.1)	1.0(±0.3)	1.0(±0.1)
τ_3 / ns	2.4(±0.6)	3.1(±0.1)	4(±1)	4(±1)
α_1^{lin} / %	21(±1)	5(±2)	58(±1)	59(±1)
α_1^{circ} / %	9(±1)	2(±1)	44.1(±0.6)	24(±1)
α_2^{lin} / %	69(±1)	61(±2)	38.9(±0.6)	39(±1)
α_2^{circ} / %	87(±4)	74(±2)	53.9(±0.7)	74(±1)
α_3^{lin} / %	10(±2)	34(±2)	3(±2)	2(±1)
α_3^{circ} / %	4(±5)	24(±2)	2(±1)	2(±1)
$\langle\tau_{\mathrm{lin}}\rangle$ / ns	1.1(±0.1)	1.8(±0.1)	0.6(±0.1)	0.6(±0.1)
$\langle\tau_{\mathrm{circ}}\rangle$ / ns	1.1(±0.2)	1.7(±0.1)	0.7(±0.2)	0.8(±0.1)

Appendix S4

Quantitative analysis of dehydrogenase reaction dynamics

The dehydrogenase reaction mechanism has been extensively studied by Callender and colleagues(13–26) and is described by the following scheme,

$$A \underset{k_{-1}}{\overset{k_1}{\rightleftharpoons}} A \cdot Eo \underset{k_{-2}}{\overset{k_2}{\rightleftharpoons}} A \cdot Eo \cdot So \underset{k_{-3}}{\overset{k_3}{\rightleftharpoons}} A \cdot Ec \cdot S \underset{k_{-4}}{\overset{k_4}{\rightleftharpoons}} B \cdot Ec \cdot P \underset{k_{-5}}{\overset{k_5}{\rightleftharpoons}} B \cdot Eo \cdot P \underset{k_{-6}}{\overset{k_6}{\rightleftharpoons}} B \cdot Eo \underset{k_{-7}}{\overset{k_7}{\rightleftharpoons}} B$$

where A is NAD(P)+, B is NAD(P)H, S is the reduced substrate (lactate or isocitrate), P is the oxidised product (pyruvate or α-ketoglutarate) and o and c represent the open and closed conformations of the enzyme E. This gives,

$$\frac{d}{dt}[A] = k_{-1}[A \cdot Eo] - k_1[A][E] \tag{S7}$$

$$\frac{d}{dt}[A \cdot Eo] = k_1[A][E] + k_{-2}[A \cdot Eo \cdot S] - k_{-1}[A \cdot Eo] - k_2[A \cdot Eo][S] \tag{S8}$$

$$\frac{d}{dt}[A \cdot Eo \cdot S] = k_2[A \cdot Eo][S] + k_{-3}[A \cdot Ec \cdot S] - k_{-2}[A \cdot Eo \cdot S] - k_3[A \cdot Eo \cdot S] \tag{S9}$$

$$\frac{d}{dt}[A \cdot Ec \cdot S] = k_3[A \cdot Eo \cdot S] + k_{-4}[B \cdot Ec \cdot P] - k_{-3}[A \cdot Ec \cdot S] - k_4[A \cdot Ec \cdot S] \tag{S10}$$

$$\frac{d}{dt}[B \cdot Ec \cdot P] = k_4[A \cdot Ec \cdot S] + k_{-5}[B \cdot Eo \cdot P] - k_{-4}[B \cdot Ec \cdot P] - k_5[B \cdot Ec \cdot P] \tag{S11}$$

$$\frac{d}{dt}[B \cdot Eo \cdot P] = k_5[B \cdot Ec \cdot P] + k_{-6}[B \cdot Eo][P] - k_{-5}[B \cdot Eo \cdot P] - k_6[B \cdot Eo \cdot P] \tag{S12}$$

$$\frac{d}{dt}[B \cdot Eo] = k_6[B \cdot Eo \cdot P] + k_{-7}[B \cdot Eo] - k_{-6}[B \cdot Eo][P] - k_7[B \cdot Eo] \tag{S13}$$

$$\frac{d}{dt}[B] = k_7[B \cdot Eo] - k_{-7}[B][E] \tag{S14}$$

The relative abundances of the fluorescent $[B \cdot Eo]$, $[B \cdot Eo \cdot P]$ and $[B \cdot Ec \cdot P]$ species for NAD- and NADP-associated enzymes would dictate the lifetimes we observe for bound NADH and bound NADPH inside cells. At steady state, these are given by,

$$\frac{[B \cdot Eo]}{[B \cdot Eo] + [B \cdot Eo \cdot P] + [B \cdot Ec \cdot P]} = \frac{1}{1 + \frac{k_{-6}}{k_6}[P] + \frac{k_{-5}}{k_5}\frac{k_{-6}}{k_6}[P]} \quad \text{(S15)}$$

$$\frac{[B \cdot Eo \cdot P]}{[B \cdot Eo] + [B \cdot Eo \cdot P] + [B \cdot Ec \cdot P]} = \frac{\frac{k_{-6}}{k_6}[P]}{1 + \frac{k_{-6}}{k_6}[P] + \frac{k_{-5}}{k_5}\frac{k_{-6}}{k_6}[P]} \quad \text{(S16)}$$

$$\frac{[B \cdot Ec \cdot P]}{[B \cdot Eo] + [B \cdot Eo \cdot P] + [B \cdot Ec \cdot P]} = \frac{\frac{k_{-5}}{k_5}\frac{k_{-6}}{k_6}[P]}{1 + \frac{k_{-6}}{k_6}[P] + \frac{k_{-5}}{k_5}\frac{k_{-6}}{k_6}[P]} \quad \text{(S17)}$$

Using temperature jump spectroscopy on lactate dehydrogenase in solution, Zhadin et al. have measured the relative rate of closing and opening of the product-bound enzyme complex k_{-5}/k_5 as 3(±2)(18). Using this value, we can plot in Figure S7 how the relative abundances of the three bound NAD(P)H species relate to the rate of association and dissociation of the product from the NAD(P)H-bound enzyme $k_{-6}[P]/k_6$.

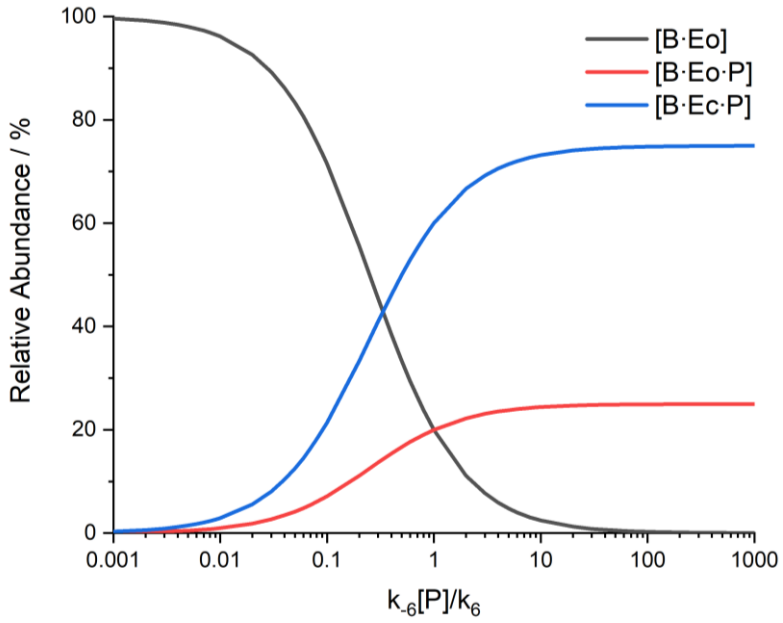

Figure S7: The relative abundance of the three bound NAD(P)H species in Equations S15 to S17 plotted as a function of the relative rate of association and dissociation of the reaction product from the enzyme, $k_{-6}[P]/k_6$, with k_{-5}/k_5 set to 3, as determined experimentally for lactate dehydrogenase.

Figure S7 demonstrates that an increased affinity of the product for the enzyme (higher $k_{-6}[P]/k_6$) leads to a greater abundance of ternary complex enzymes. In our measurements, only the closed conformation of these had a lifetime large enough to reflect the 4.4(±0.2)ns fluorescence lifetime of intracellular bound NADPH. This implies that $k_{-6}[P]/k_6$ is greater for NADPH- than NADH-associated dehydrogenases inside cells.

We note that, as $k_{-6}[P]/k_6 \to \infty$, the relative proportion of $[B \cdot Eo \cdot P]$ and $[B \cdot Ec \cdot P]$ asymptotically approach 25% and 75% respectively. Our measurements suggest these two species would have lifetimes of 1.7ns and 5.3ns for NADPH, giving a concentration weighted average lifetime of 4.4 ns, in exact agreement with our estimate of the fluorescence lifetime of bound NADPH inside cells. In contrast, as $k_{-6}[P]/k_6 \to 0$, the relative proportion of the $[B \cdot Eo]$ species approaches 100%. For NADH, our measurements suggest this corresponds to a lifetime of 1.34ns, within the 0.2ns error bounds of our 1.5ns estimate for its bound intracellular fluorescence lifetime.

Measurements on lactate dehydrogenase(27) have determined a value of $k_{-6}/k_6 = 1.1(\pm 0.4)$ x 10^4 M^{-1} in solution(18). At $[P] = 239$ µM, based on previous cellular pyruvate measurements, the relative weightings of the $[B \cdot Eo]$, $[B \cdot Eo \cdot P]$ and $[B \cdot Ec \cdot P]$ species would be 8.7%, 22.8% and 68.5% according to Equations S15 to S17. Using the lifetime values we measured for each species, these relative proportions would give an average bound lifetime for NADH of 3.0ns, much larger than that we observed inside living cells. This implies that one or more of the rates measured in solution may not apply inside the cell for NADH-associated reactions. k_{-5}, k_5 and k_6 may be more likely to be valid, given that they concern internal transitions within the protein rather than interactions with the environment. There is, however, a growing consensus that constants such as k_{-6}, governing diffusion-limited processes, can be substantially different within the complex, crowded and viscous intracellular milieu(28–33).

An alternative explanation for this disagreement is the neglect of two potentially significant phenomena by this model. Firstly, while the measurements we performed on ternary complexes utilised reduced substrates to ensure no oxidation of NADH and NADPH, there is evidence that the oxidised substrates (e.g. pyruvate, α-ketoglutarate) can quench the fluorescence of the reduced cofactors by providing an acceptor for photoinduced electron transfer(25). This would result in a fluorescence lifetime smaller than that we measured for NAD(P)H in ternary complex with the reduced substrate. Secondly, the model includes only the chain of configurations participating in the catalytic process of the enzyme, but catalytically unproductive configurations can also occur. The binding of reduced substrates alongside reduced cofactors (the so-called "abortive complex") plays a significant role in the regulation of dehydrogenases(34, 35), and the closed enzyme configuration can occur in the absence of substrate, blocking its binding(26). We therefore integrated these phenomena into our model by adding the side reactions,

$$A \cdot Eo \underset{k_{-i}}{\overset{k_i}{\rightleftharpoons}} A \cdot Eo \cdot P \underset{k_{-j}}{\overset{k_j}{\rightleftharpoons}} A \cdot Ec \cdot P$$

$$A \cdot Eo \underset{k_{-k}}{\overset{k_k}{\rightleftharpoons}} A \cdot Ec$$

$$B \cdot Eo \underset{k_{-x}}{\overset{k_x}{\rightleftharpoons}} B \cdot Eo \cdot S \underset{k_{-y}}{\overset{k_y}{\rightleftharpoons}} B \cdot Ec \cdot S$$

$$B \cdot Eo \underset{k_{-z}}{\overset{k_z}{\rightleftharpoons}} B \cdot Ec$$

Repeating the steady state analysis as above gives the following relative weighting for the six different bound NAD(P)H species,

$$\frac{[B \cdot Eo]}{[B \cdot Eo] + [B \cdot Eo \cdot P] + [B \cdot Eo \cdot S] + [B \cdot Ec \cdot P] + [B \cdot Ec \cdot S] + [B \cdot Ec]} = \frac{1}{1 + \frac{k_{-6}}{k_6}[P] + \frac{k_x}{k_{-x}}[S] + \frac{k_{-5}}{k_5}\frac{k_{-6}}{k_6}[P] + \frac{k_x}{k_{-x}}\frac{k_y}{k_{-y}}[S] + \frac{k_z}{k_{-z}}} \quad \text{(S18)}$$

$$\frac{[B \cdot Eo \cdot P]}{[B \cdot Eo] + [B \cdot Eo \cdot P] + [B \cdot Eo \cdot S] + [B \cdot Ec \cdot P] + [B \cdot Ec \cdot S] + [B \cdot Ec]} = \frac{\frac{k_{-6}}{k_6}[P]}{1 + \frac{k_{-6}}{k_6}[P] + \frac{k_x}{k_{-x}}[S] + \frac{k_{-5}}{k_5}\frac{k_{-6}}{k_6}[P] + \frac{k_x}{k_{-x}}\frac{k_y}{k_{-y}}[S] + \frac{k_z}{k_{-z}}} \quad \text{(S19)}$$

$$\frac{[B \cdot Eo \cdot S]}{[B \cdot Eo] + [B \cdot Eo \cdot P] + [B \cdot Eo \cdot S] + [B \cdot Ec \cdot P] + [B \cdot Ec \cdot S] + [B \cdot Ec]} = \frac{\frac{k_x}{k_{-x}}[S]}{1 + \frac{k_{-6}}{k_6}[P] + \frac{k_x}{k_{-x}}[S] + \frac{k_{-5}}{k_5}\frac{k_{-6}}{k_6}[P] + \frac{k_x}{k_{-x}}\frac{k_y}{k_{-y}}[S] + \frac{k_z}{k_{-z}}} \quad \text{(S20)}$$

$$\frac{[B \cdot Ec \cdot P]}{[B \cdot Eo] + [B \cdot Eo \cdot P] + [B \cdot Eo \cdot S] + [B \cdot Ec \cdot P] + [B \cdot Ec \cdot S] + [B \cdot Ec]} = \frac{\frac{k_{-5}}{k_5}\frac{k_{-6}}{k_6}[P]}{1 + \frac{k_{-6}}{k_6}[P] + \frac{k_x}{k_{-x}}[S] + \frac{k_{-5}}{k_5}\frac{k_{-6}}{k_6}[P] + \frac{k_x}{k_{-x}}\frac{k_y}{k_{-y}}[S] + \frac{k_z}{k_{-z}}} \quad \text{(S21)}$$

$$\frac{[B \cdot Ec \cdot S]}{[B \cdot Eo] + [B \cdot Eo \cdot P] + [B \cdot Eo \cdot S] + [B \cdot Ec \cdot P] + [B \cdot Ec \cdot S] + [B \cdot Ec]} = \frac{\frac{k_x}{k_{-x}}\frac{k_y}{k_{-y}}[S]}{1 + \frac{k_{-6}}{k_6}[P] + \frac{k_x}{k_{-x}}[S] + \frac{k_{-5}}{k_5}\frac{k_{-6}}{k_6}[P] + \frac{k_x}{k_{-x}}\frac{k_y}{k_{-y}}[S] + \frac{k_z}{k_{-z}}} \quad \text{(S22)}$$

$$\frac{[B \cdot Ec]}{[B \cdot Eo] + [B \cdot Eo \cdot P] + [B \cdot Eo \cdot S] + [B \cdot Ec \cdot P] + [B \cdot Ec \cdot S] + [B \cdot Ec]} = \frac{\frac{k_z}{k_{-z}}}{1 + \frac{k_{-6}}{k_6}[P] + \frac{k_x}{k_{-x}}[S] + \frac{k_{-5}}{k_5}\frac{k_{-6}}{k_6}[P] + \frac{k_x}{k_{-x}}\frac{k_y}{k_{-y}}[S] + \frac{k_z}{k_{-z}}} \quad \text{(S23)}$$

To simplify this preliminary analysis, we assume that the rates governing the transition between open and closed enzyme states are equal in the presence of both (oxidised) products $[P]$ and (reduced) substrates $[S]$ ($k_y/k_{-y} = k_{-5}/k_5$) and that the rates of binding and unbinding of product and substrate to the open conformation NAD(P)H-bound enzyme are equal ($k_x/k_{-x} = k_{-6}/k_6$). We will also assume that the fluorescence lifetimes of NAD(P)H in the open conformation ternary complexes are identical, regardless of whether product or substrate is bound. Finally, to relate the relative proportions of each species back to the contrasting intracellular biochemistry of the NAD and NADP pools, we will replace the relative concentrations of $[P]$ and $[S]$ with the redox balance of the associated cofactor pool using the equilibrium constant(36, 37),

$$\frac{[P]}{[S]} = K_{\mathrm{eq}} \frac{[A]}{[B]} \tag{S24}$$

Introducing these simplifications into Equations S18 to S23, writing the total concentration of substrates and products as $[T]$, gives,

$$\frac{[B \cdot Eo]}{[B \cdot Eo] + [B \cdot Eo \cdot P] + [B \cdot Eo \cdot S] + [B \cdot Ec \cdot P] + [B \cdot Ec \cdot S] + [B \cdot Ec]} = \frac{\frac{1}{[T]}}{\frac{1}{[T]}\left(1 + \frac{k_z}{k_{-z}}\right) + \frac{k_{-6}}{k_6}\left(1 + \frac{k_{-5}}{k_5}\right)} \tag{S25}$$

$$\frac{[B \cdot Eo \cdot P] + [B \cdot Eo \cdot S]}{[B \cdot Eo] + [B \cdot Eo \cdot P] + [B \cdot Eo \cdot S] + [B \cdot Ec \cdot P] + [B \cdot Ec \cdot S] + [B \cdot Ec]} = \frac{\frac{k_{-6}}{k_6}}{\frac{1}{[T]}\left(1 + \frac{k_z}{k_{-z}}\right) + \frac{k_{-6}}{k_6}\left(1 + \frac{k_{-5}}{k_5}\right)} \tag{S26}$$

$$\frac{[B \cdot Ec \cdot P]}{[B \cdot Eo] + [B \cdot Eo \cdot P] + [B \cdot Eo \cdot S] + [B \cdot Ec \cdot P] + [B \cdot Ec \cdot S] + [B \cdot Ec]}$$

$$= \frac{\frac{k_{-5}}{k_5}\frac{k_{-6}}{k_6}\left(\frac{K_{\mathrm{eq}}\,[A]/[B]}{1 + K_{\mathrm{eq}}\,[A]/[B]}\right)}{\frac{1}{[T]}\left(1 + \frac{k_z}{k_{-z}}\right) + \frac{k_{-6}}{k_6}\left(1 + \frac{k_{-5}}{k_5}\right)} \quad \text{(S27)}$$

$$\frac{[B \cdot Ec \cdot S]}{[B \cdot Eo] + [B \cdot Eo \cdot P] + [B \cdot Eo \cdot S] + [B \cdot Ec \cdot P] + [B \cdot Ec \cdot S] + [B \cdot Ec]}$$

$$= \frac{\frac{k_{-5}}{k_5}\frac{k_{-6}}{k_6}\left(\frac{1}{1 + K_{\mathrm{eq}}\,[A]/[B]}\right)}{\frac{1}{[T]}\left(1 + \frac{k_z}{k_{-z}}\right) + \frac{k_{-6}}{k_6}\left(1 + \frac{k_{-5}}{k_5}\right)} \quad \text{(S28)}$$

$$\frac{[B \cdot Ec]}{[B \cdot Eo] + [B \cdot Eo \cdot P] + [B \cdot Eo \cdot S] + [B \cdot Ec \cdot P] + [B \cdot Ec \cdot S] + [B \cdot Ec]}$$

$$= \frac{\frac{1}{[T]}\frac{k_z}{k_{-z}}}{\frac{1}{[T]}\left(1 + \frac{k_z}{k_{-z}}\right) + \frac{k_{-6}}{k_6}\left(1 + \frac{k_{-5}}{k_5}\right)} \quad \text{(S29)}$$

In Figure S8, we plot Equations S25 to S29 as a function of $K_{\mathrm{eq}}\,[A]/[B]$ to understand how the redox balance of the cofactor pool may relate to the relative abundances of each enzyme bound species. k_{-5}/k_5 and k_{-6}/k_6 were set at 3 and 1.1 x 10^4 M^{-1} respectively, based on the experimental measurements described above(18). k_z/k_{-z} was estimated as 0.095, an average of the 0.04 and 0.15 values of the α_3/α_2 ratios in our binary complex measurements for NADH and NADPH. The concentration scale $[T]$ was chosen as 1mM to reflect the order of magnitude of intracellular redox couples(27).

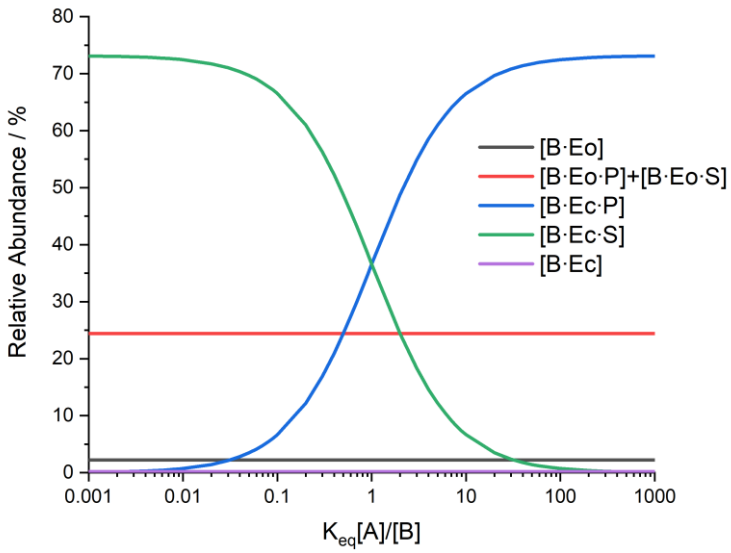

Figure S8: The relative abundance of the five bound NAD(P)H species in Equations S25 to S29 plotted against the product of the NAD(P) redox balance, $[A]/[B]$, and the equilibrium constant K_{eq}. k_{-5}/k_5 and k_{-6}/k_6 were set to the values of 3 and 1.1 x 10^4 M^{-1} respectively, as determined experimentally for lactate dehydrogenase(18). k_z/k_{-z} was set to 0.095, the average of the α_3/α_2 ratios in our measurements of NADH and NADPH in binary complexes. The concentration scale $[T]$ was set to 1mM.

Figure S8 demonstrates that the contributions from open and closed binary complexes remain constant with cofactor redox state, at 2.2% and 0.2% respectively. This is also the case for the combined contribution from open ternary complexes, remaining at 24.4%; a consequence of assuming the fluorescence lifetime of the cofactor to be invariant to the presence of oxidised product or reduced substrate molecules in the open conformation. In contrast, the abortive ternary complex of NAD(P)H with reduced substrate dominates at low values of $K_{\mathrm{eq}}[A]/[B]$, whereas the catalytic ternary complex of NAD(P)H with the oxidised product dominates at high values of $K_{\mathrm{eq}}[A]/[B]$. This could provide a possible mechanism for the difference in the enzyme bound lifetime of NADPH and NADH inside cells where the NADP redox state is

maintained low ($[A]/[B] \ll 1$) and the NAD redox state is maintained high ($[A]/[B] \gg 1$)(36, 38).

In the limit of $K_{\mathrm{eq}}[A]/[B] \to 0$, the contribution from the closed ternary complex with oxidised product goes to zero, corresponding to a concentration-weighted mean bound lifetime of 4.3ns using the fluorescence lifetimes obtained in our experiments on NADPH and isocitrate dehydrogenase (1.6, 1.7, 5.3 and 4.37ns for $[B \cdot Eo]$, $[B \cdot Eo \cdot P] + [B \cdot Eo \cdot S]$, $[B \cdot Ec \cdot S]$ and $[B \cdot Ec]$ respectively). This is within the 0.2ns error bounds of our estimate of the fluorescence lifetime of bound NADPH inside cells of 4.4ns. Given our lack of knowledge of the fluorescence lifetime of NADH in complex with an oxidised product (e.g. pyruvate), it is not possible to carry out similar calculations for $K_{\mathrm{eq}}[A]/[B] \to \infty$. However, to achieve a concentration weighted average lifetime equal to the 1.5ns fluorescence lifetime of bound NADH inside cells, the fluorescence lifetimes obtained in our experiments on NADH and lactate dehydrogenase (1.34, 1.9 and 3.19ns for $[B \cdot Eo]$, $[B \cdot Eo \cdot P] + [B \cdot Eo \cdot S]$ and $[B \cdot Ec]$ respectively) would require excited state quenching by oxidised products to decrease the lifetime of ternary complex NADH to 1.37ns. Relative to the 3.64 ns lifetime of NADH in ternary complex with lactate, this would require a rate of photoinduced electron transfer of 0.46 ns^{-1}, within the range expected for biomolecular systems(39, 40).

It is important to note that these basic models are based on best guesses for the rate constants and neglect any differences in these parameters between NADH- and NADPH-associated enzymes. Nevertheless, they allow a preliminary analysis of the effect of the differing redox states of the NAD and NADP pools on the equilibria of the NAD(P)H-bound enzyme conformations, revealing that the low NADP+/NADPH ratio results in a larger fluorescence lifetime for bound NADPH than bound NADH at a given value of the equilibrium constant due to the increased proportion of abortive ternary complexes.

Supplemental References

1. Hanley, Q.S., V. Subramaniam, D.J. Arndt-Jovin, and T.M. Jovin. 2001. Fluorescence Lifetime Imaging: Multi-point Calibration, Minimum Resolvable Differences, and Artifact Suppression. *Cytometry*. 43:248–260.

2. Teegarden, K.J. 1957. Luminescence of potassium iodide. *Phys. Rev.* 105:1222–1227.

3. Maus, M., M. Cotlet, J. Hofkens, T. Gensch, F.C. De Schryver, J. Schaffer, and C.A.M. Seidel. 2001. An experimental comparison of the maximum likelihood estimation and nonlinear least-squares fluorescence lifetime analysis of single molecules. *Anal. Chem.* 73:2078–2086.

4. Bevington, P.R., and D.K. Robinson. 2003. Data Reduction and Error Analysis for the Physical Sciences. 3rd Edition. McGraw-Hill.

5. Taylor, J. 1997. Introduction to error analysis, the study of uncertainties in physical measurements. University Science Books.

6. Bajzer, Ž., T.M. Therneau, J.C. Sharp, and F.G. Prendergast. 1991. Maximum likelihood method for the analysis of time-resolved fluorescence decay curves. *Eur. Biophys. J.* 20:247–262.

7. Santra, K., J. Zhan, X. Song, E.A. Smith, N. Vaswani, and J.W. Petrich. 2016. What Is the Best Method to Fit Time-Resolved Data? A Comparison of the Residual Minimization and the Maximum Likelihood Techniques As Applied to Experimental Time-Correlated, Single-Photon Counting Data. *J. Phys. Chem. B.* 120:2484–2490.

8. Köllner, M., and J. Wolfrum. 1992. How many photons are necessary for fluorescence-lifetime measurements? *Chem. Phys. Lett.* 200:199–204.

9. Blacker, T.S., R.J. Marsh, M.R. Duchen, and A.J. Bain. 2013. Activated barrier crossing

dynamics in the non-radiative decay of NADH and NADPH. *Chem. Phys.* 422:184–194.

10. Ebbinghaus, S., J.K. Seung, M. Heyden, X. Yu, U. Heugen, M. Gruebele, D.M. Leitner, and M. Havenith. 2007. An extended dynamical hydration shell around proteins. *Proc. Natl. Acad. Sci. U. S. A.* 104:20749–20752.

11. Xu, X., J. Zhao, Z. Xu, B. Peng, Q. Huang, E. Arnold, and J. Ding. 2004. Structures of human cytosolic NADP-dependent isocitrate dehydrogenase reveal a novel self-regulatory mechanism of activity. *J. Biol. Chem.* 279:33946–33957.

12. Friberg, A., H. Rehwinkel, D. Nguyen, V. Pütter, M. Quanz, J. Weiske, U. Eberspächer, I. Heisler, and G. Langer. 2020. Structural Evidence for Isoform-Selective Allosteric Inhibition of Lactate Dehydrogenase A. *ACS Omega*. 5:13034–13041.

13. Deng, H., N. Zhadin, and R. Callender. 2001. Dynamics of protein ligand binding on multiple time scales: NADH binding to lactate dehydrogenase. *Biochemistry*. 40:3767–3773.

14. Deng, H., S. Brewer, D.M. Vu, K. Clinch, R. Callender, and R.B. Dyery. 2008. On the pathway of forming enzymatically productive ligand-protein complexes in lactate dehydrogenase. *Biophys. J.* 95:804–813.

15. Reddish, M.J., H.L. Peng, H. Deng, K.S. Panwar, R. Callender, and R.B. Dyer. 2014. Direct evidence of catalytic heterogeneity in lactate dehydrogenase by temperature jump infrared spectroscopy. *J. Phys. Chem. B.* 118:10854–10862.

16. Reddish, M.J., R. Callender, and R.B. Dyer. 2017. Resolution of Submillisecond Kinetics of Multiple Reaction Pathways for Lactate Dehydrogenase. *Biophys. J.* 112:1852–1862.

17. Zhadin, N., and R. Callender. 2011. Effect of osmolytes on protein dynamics in the lactate dehydrogenase- catalyzed reaction. *Biochemistry*. 50:1582–1589.

18. Zhadin, N., M. Gulotta, and R. Callender. 2008. Probing the role of dynamics in hydride transfer catalyzed by lactate dehydrogenase. *Biophys. J.* 95:1974–1984.

19. Deng, H., D. V. Vu, K. Clinch, R. Desamero, R.B. Dyer, and R. Callender. 2011. Conformational heterogeneity within the Michaelis complex of lactate dehydrogenase. *J. Phys. Chem. B.* 115:7670–7678.

20. Gulotta, M., H. Deng, H. Deng, R.B. Dyer, and R.H. Callender. 2002. Toward an understanding of the role of dynamics on enzymatic catalysis in lactate dehydrogenase. *Biochemistry*. 41:3353–3363.

21. McClendon, S., N. Zhadin, and R. Callender. 2005. The approach to the Michaelis complex in lactate dehydrogenase: The substrate binding pathway. *Biophys. J.* 89:2024–2032.

22. McClendon, S., D.M. Vu, K. Clinch, R. Callender, and R.B. Dyer. 2005. Structural transformations in the dynamics of Michaelis complex formation in lactate dehydrogenase. *Biophys. J.* 89:L07–L09.

23. Peng, H.L., H. Deng, R.B. Dyer, and R. Callender. 2014. Energy landscape of the michaelis complex of lactate dehydrogenase: Relationship to catalytic mechanism. *Biochemistry*. 53:1849–1857.

24. Pineda, J.R.E.T., R. Callender, and S.D. Schwartz. 2007. Ligand binding and protein dynamics in lactate dehydrogenase. *Biophys. J.* 93:1474–1483.

25. Peng, H.L., and R. Callender. 2017. Mechanistic Analysis of Fluorescence Quenching of Reduced Nicotinamide Adenine Dinucleotide by Oxamate in Lactate Dehydrogenase Ternary Complexes. *Photochem. Photobiol.* 93:1193–1203.

26. Qiu, L., M. Gulotta, and R. Callender. 2007. Lactate dehydrogenase undergoes a substantial structural change to bind its substrate. *Biophys. J.* 93:1677–1686.

27. Tischler, M.E., D. Friedrichs, K. Coll, and J.R. Williamson. 1977. Pyridine nucleotide distributions and enzyme mass action ratios in hepatocytes from fed and starved rats. *Arch. Biochem. Biophys.* 184:222–236.

28. Matić, M., S. Saurabh, J. Hamacek, and F. Piazza. 2020. Crowding-Induced Uncompetitive Inhibition of Lactate Dehydrogenase: Role of Entropic Pushing. *J. Phys. Chem. B.* 124:727–734.

29. Wilcox, A.E., M.A. LoConte, and K.M. Slade. 2016. Effects of macromolecular crowding on alcohol dehydrogenase activity are substrate-dependent. *Biochemistry*. 55:3550–3558.

30. Zheng, K., T.P. Jensen, L.P. Savtchenko, J.A. Levitt, K. Suhling, and D.A. Rusakov. 2017. Nanoscale diffusion in the synaptic cleft and beyond measured with time-resolved fluorescence anisotropy imaging. *Sci. Rep.* 7:42022.

31. Molines, A.T., J. Lemière, M. Gazzola, I.E. Steinmark, C.H. Edrington, C.T. Hsu, P. Real-Calderon, K. Suhling, G. Goshima, L.J. Holt, M. Thery, G.J. Brouhard, and F. Chang. 2022. Physical properties of the cytoplasm modulate the rates of microtubule polymerization and depolymerization. *Dev. Cell*. 57:466-479.e6.

32. Ellis, R.J. 2001. Macromolecular crowding: An important but neglected aspect of the intracellular environment. *Curr. Opin. Struct. Biol.* 11:114–119.

33. Minton, A.P. 2006. How can biochemical reactions within cells differ from those in test tubes? *J. Cell Sci.* 119:2863–2869.

34. Fromm, H. 1963. Determination of Dissociation Constants of Coenzymes and Abortive. *J. Biol. Chem.* 238:2938–2944.

35. Eggert, M.W., M.E. Byrne, and R.P. Chambers. 2011. Impact of high pyruvate concentration on kinetics of rabbit muscle lactate dehydrogenase. *Appl. Biochem.*

Biotechnol. 165:676–686.

36. Veech, R.L., L. V. Eggleston, and H.A. Krebs. 1969. The redox state of free nicotinamide-adenine dinucleotide phosphate in the cytoplasm of rat liver. *Biochem. J.* 115:609–619.

37. Williamson, D.H., P. Lund, and H.A. Krebs. 1967. The redox state of free nicotinamide-adenine dinucleotide in the cytoplasm and mitochondria of rat liver. *Biochem. J.* 103:514–527.

38. Sun, F., C. Dai, J. Xie, and X. Hu. 2012. Biochemical issues in estimation of cytosolic free NAD/NADH ratio. *PLoS One.* 7:e34525.

39. Van Den Berg, P.A.W., A. Van Hoek, C.D. Walentas, R.N. Perham, and A.J.W.G. Visser. 1998. Flavin fluorescence dynamics and photoinduced electron transfer in Escherichia coli glutathione reductase. *Biophys. J.* 74:2046–2058.

40. Piotrowiak, P. 1999. Photoinduced electron transfer in molecular systems: Recent developments. *Chem. Soc. Rev.* 28:143–150.